

Multimodal and Multiscale Deep Neural Networks for the Early Diagnosis of Alzheimer's Disease using structural MR and FDG-PET images

Donghuan Lu^{1,*}, Karteek Popuri¹, Weiguang Ding¹, Rakesh Balachandar¹, Mirza Faisal Beg¹, and for the Alzheimer's Disease Neuroimaging Initiative⁺

¹School of Engineering Science, Simon Fraser University, Burnaby, V5A 1S6, Canada

*ludonghuan9@gmail.com

⁺Data used in preparation of this article were obtained from the Alzheimer's Disease Neuroimaging Initiative (ADNI) database (adni.loni.usc.edu). As such, the investigators within the ADNI contributed to the design and implementation of ADNI and/or provided data but did not participate in analysis or writing of this report. A complete listing of ADNI investigators can be found at: http://adni.loni.usc.edu/wp-content/uploads/how_to_apply/ADNI_Acknowledgement_List.pdf

ABSTRACT

Alzheimer's Disease (AD) is a progressive neurodegenerative disease. Amnesic mild cognitive impairment (MCI) is a common first symptom before the conversion to clinical impairment where the individual becomes unable to perform activities of daily living independently. Although there is currently no treatment available, the earlier a conclusive diagnosis is made, the earlier the potential for interventions to delay or perhaps even prevent progression to full-blown AD. Neuroimaging scans acquired from MRI and metabolism images obtained by FDG-PET provide in-vivo view into the structure and function (glucose metabolism) of the living brain. It is hypothesized that combining different image modalities could better characterize the change of human brain and result in a more accuracy early diagnosis of AD. In this paper, we proposed a novel framework to discriminate normal control(NC) subjects from subjects with AD pathology (AD and NC, MCI subjects convert to AD in future). Our novel approach utilizing a multimodal and multiscale deep neural network was found to deliver a 85.68% accuracy in the prediction of subjects within 3 years to conversion. Cross validation experiments proved that it has better discrimination ability compared with results in existing published literature.

Introduction

Alzheimer's disease (AD), the most common dementia, affecting 1 out of 9 people over the age of 65 years¹. Alzheimer's diseases involves progressive cognitive impairment, commonly associated with early memory loss, requiring assistance for activities of self care during advanced stages. Alzheimer's is posited to evolve through a prodromal stage which is commonly referred to as the mild cognitive impairment(MCI) stage and 10 - 15% of individuals with MCI, progress to AD² each year. With improved life expectancy, it is estimated that about 1.2% of global population will develop Alzheimer's disease by 2046³ thereby affecting millions of individuals directly, as well as many more indirectly through the effects on their families and caregivers. Current Alzheimer's research targets reliable prodromal identification of patients harbouring Alzheimer's pathology, for reasons that early intervention could potentially change the course of illness. Clinical diagnosis involves rigorous evaluation to rule out non-Alzheimer's causes for cognitive decline but this is however limited by specificity of identifying prodromal AD. Hence, we see the necessity of a tool to reliably detect and identify prodromal Alzheimer's disease.

Efforts to understand AD pathology in the past resulted in identifying neuroimaging as one of the promising tool for prodromal diagnosis⁴. Neuroimaging involving magnetic resonance imaging (MRI)⁵ and fluorodeoxyglucose positron emission tomography (FDG-PET)⁶ were the unique imaging modalities recognized as useful tools to identify individuals with prodromal AD. MRI offers structural details such as texture, thickness, density and shape of various brain regions, while FDG-PET measures the resting state glucose metabolism⁷, reflecting the functional activity of the underlying tissue⁶. FDG-PET and MRI are frequently employed neuroimaging techniques in computer-aided diagnosis of neurodegenerative diseases. There has been considerable efforts to use structural MRI⁸⁻¹⁰ or FDG-PET^{11,12} or a combination with other biomarkers^{13,14} to develop automated computer aided tools for prodromal diagnosis of Alzheimer's disease.

Deep neural networks have been studied extensively and proven to have the best performance for many recognition tasks¹⁵. The application of deep neural networks in recognition of AD-related patterns has also attracted interests in its application for

prodromal AD¹⁶⁻¹⁸. By applying deep neural network to extract features, such as stacked autoencoder(SAE) or Deep Boltzmann Machine(DBM), these approaches outperform other popular machine learning methods, e.g., support vector machine (SVM) and random forest techniques. However, one of the major hurdles preventing applications of deep learning in neuroimaging is that it requires a large data set to train the model, while the available number of images are limited to several hundred or thousand which are much less than feature dimension of data sample. To overcome this challenge, one popular approach is to segment images into patches and extract features from each patch¹⁶⁻¹⁸. However, down sampling the input data can result in the loss of discriminative information which could be a potential reason why previous methods haven't achieved satisfying accuracy for this diagnostic task. A common extension to pattern mining and feature extraction for image recognition is multiscale processing^{19,20}. By extracting features at different resolutions or scales, multiscale features can better characterize images for classification task and a recent study indicates it can also improve the classification performance of deep neural networks²¹.

Therefore, we are proposing a novel approach to combine multiscale and multimodal processing with deep neural network for the early diagnosis of AD. Through cross validation experiments with more than 1000 subjects, we demonstrated that 1) our network can learn hidden patterns from multiscale and multimodal features for the detection of AD pathology; 2) our approach outperform previous methods regarding the discriminative task of potential AD subjects; and, 3) our network can identify the subjects who are going to convert to AD in 3 years with an accuracy of 85.68% which is a promising result.

Methods

There are two major steps in the proposed framework: 1)image preprocessing: segment both MRI scans and FDG-PET images into patches, and extract features from each patch; and, 2)classification: train a deep neural network to learn the patterns that discriminate AD pathology, and then use it to classify individuals with AD pathology.

Data

Data used in the preparation of this article were obtained from the Alzheimer's Disease Neuroimaging Initiative (ADNI) database (adni.loni.usc.edu). The ADNI was launched in 2003 as a public-private partnership, led by Principal Investigator Michael W. Weiner, MD. The primary goal of ADNI has been to test whether serial MRI, PET, other biological markers, and clinical and neuropsychological assessment can be combined to measure the progression of mild cognitive impairment (MCI) and early Alzheimer's disease (AD).

For a comprehensive validation of the proposed method, it is emphasized that all the available ADNI subjects(N = 1242) with both a T1-weighted MRI scan and FDG-PET image at the time of preparation of this manuscript were used in this study. These subjects were categorized into 5 groups: 1) stable Normal controls (sNC): 360 subjects diagnosed to be NC at baseline and remained the same at the time of preparation of this manuscript; 2) stable MCI (sMCI): 409 subjects diagnosed to be MCI at all time points(at least for 2 years); 3) progressive NC (pNC): 18 subjects evaluated to be NC at baseline but have progressed to probable AD at the time of preparation of this manuscript; 4) progressive MCI (pMCI): 217 subjects evaluated to be MCI at baseline and progressed to probable AD; 5) stable Alzheimer's disease (sAD): 238 subjects diagnosed to be AD for all available time points. Demographic and clinical information of the subjects are shown in Table 1. Numbers in brackets are the number of male and female subjects in the second row, while in the rest 3 rows the two number represent the minimum and maximum value of age, education year and MMSE(Mini-Mental State Examination) score. It was worth mentioning that each subject could have multiple scans at different time points. In total there were 2402 FDG-PET scans and 2402 MRI images used in this study. Detailed descriptions of the ADNI subject cohorts, image acquisition protocols procedures and post-acquisition preprocessing procedures can be found at <http://www.adni-info.org>.

Mean(min-max)	sNC	sMCI	pNC	pMCI	sAD
Count (M/F)	360(167/193)	409(239/170)	18(11/7)	217(126/91)	238(141/97)
Age	73.4(60-94)	74(56-91)	77(68-84)	74(55-89)	75(55-90)
Education	16.5(6-20)	15.8(7-20)	15.7(12-20)	16.0(8-20)	15.3(4-20)
MMSE	29.1(24-30)	28.0(22-30)	29.4(27-30)	26.5(9-30)	23.2(18-27)

Table 1. Subject Demographics. In the second row, the first number in each cell is the total number of subjects and the numbers in brackets represents the number of male and female. In the last 3 rows, the first number in each cell is the mean and the two numbers in brackets are the minimum and maximum value of age, education year and MMSE score, respectively.

Image Processing

Unlike typical image recognition problems where deep learning has shown to be effective, our data set is relatively small. Hence directly using this smaller database of images to train the deep neural network is not likely to deliver high classification accuracy.

However, contrary to typical image recognition tasks, where the images contain large heterogeneity, the images in this database are all human brain images acquired with similar pose and scale which show relatively much less heterogeneity in comparison. Therefore we applied following processing steps to extract patch-wise features as shown in Figure 1: FreeSurfer 5.1²² was used to segment each T1 structural MRI image into gray matter and white matter followed by subdivision of the gray matter into 87 anatomical regions of interest (ROI). The FreeSurfer segmentation were quality controlled by an expert neuroanatomist and any errors noted were manually corrected. Then, for a standard T1 MRI image, a voxel-wise k -means clustering based on spatial coordinates was performed to segment each ROI into patches based on its spatial information²³. The size of patch was predefined as 500, 1000 and 2000 voxels in this study and resulted into 1488, 705 and 343 patches, respectively. It was designed to keep enough detailed information as well as avoiding too large feature dimension considering the limited number of data samples were available in this study. Subsequently, each ROI of the standard template MRI was registered to the same ROI of every target image via a high-dimensional non-rigid registration method (LDDMM²⁴). The registration maps were then applied to the patch-wise segmentation of the standard template. This transformed the template segmentation into each target MRI space so the target images were subdivided into the same number of patches. It worth mentioning that after the transformation, the size of a template patch in different images is not the same due to non-rigid registration encoding local expansion/contraction and hence is one of the features used to represent the regional information of a given structural brain scan. Then, for each target subject, the FDG-PET image of the subject was co-registered to its skull-stripped T1 MRI scan with a rigid transformation using FSL-FLIRT program²⁵ based on normalized mutual information. The degrees of freedom (DOF) was set as 12 and Normalized correlation was used as cost function. The mean intensity in the brainstem region of the FDG-PET image was the chosen reference to normalize the voxel intensities in that individual brain metabolism image, because brainstem region was most unlikely to be affected by AD. The mean intensity of each patch was used as an element to form the feature vector to represent the metabolism activity, and the volume of each patch was used to represent the brain atrophy.

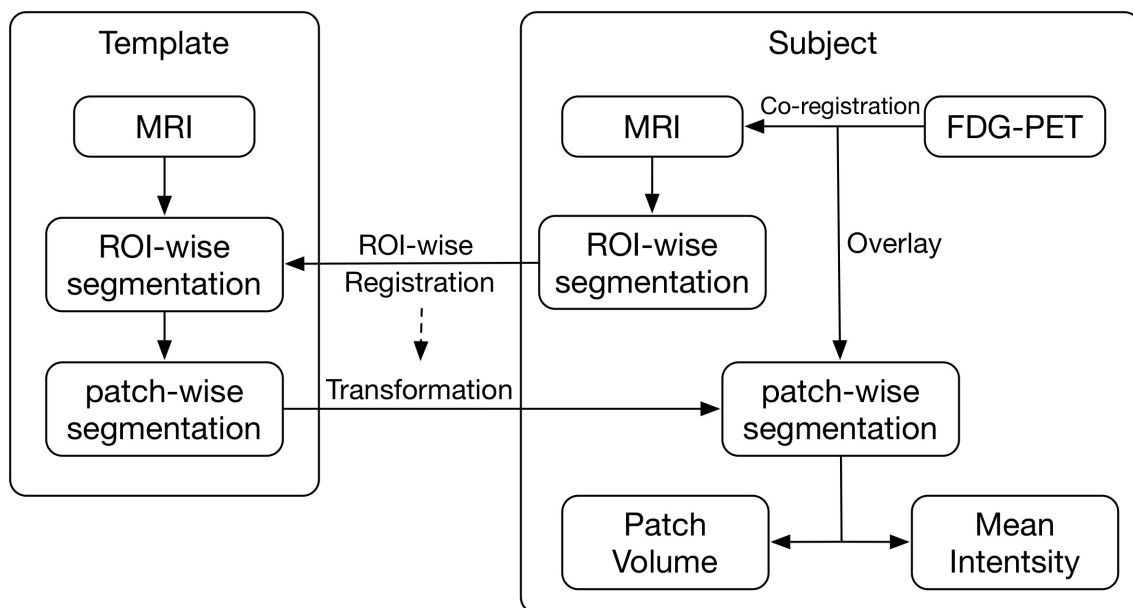


Figure 1. Flowchart of extracting patch-wise features from MRI scans and FDG-PET images. Each subject was segmented into patches through registration to a segmented template. Patch volume and mean intensity of FDG-PET were extracted as the feature to represent each patch.

Multiscale Deep Neural Network

With the features extracted from MRI and FDG-PET images, we trained a Multimodal Multiscale Deep Neural Network (MMDNN) to perform the classification. As shown in Fig 2, the network consists of two parts. The first part was 6 independent deep neural network (DNN) corresponding to each scale of a single modality. The second part was another DNN used to fuse the features extracted from these 6 DNNs. The input data of this DNN was the concatenated latent representation learned from each single DNN. The DNNs in two parts shared the same structure. For each DNN, the number of nodes for each hidden layer were set as $3N$, $\frac{3}{4}N$ and 100 respectively, where N denotes the dimension of input feature vector. The number of nodes was chosen to explore all possible hidden correlation across features from different patches in the first layer and gradually reduce the number of features in the following layers to avoid over-fitting. We trained each DNN with two steps, unsupervised

pre-training and supervised fine-tuning, respectively. Then all the parameters of MMDNN was tuned together.

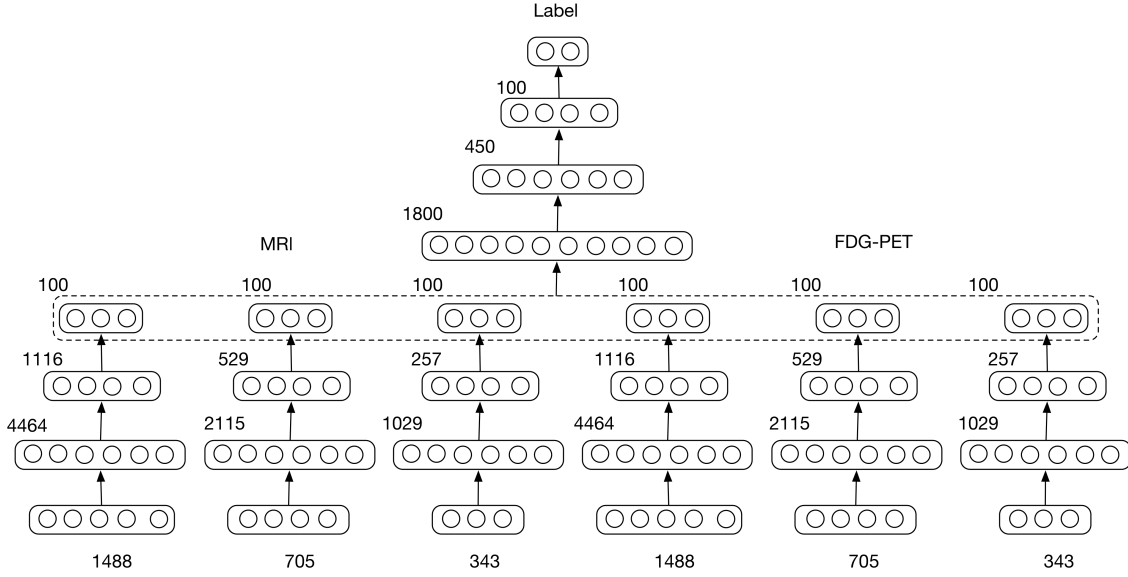


Figure 2. Multimodal Multiscale Deep Neural Network. 1488, 705 and 343 are input feature dimension(number of patches) extracted from different scales. For each layer, its number of nodes was denoted by the number on its top left. For each scale of each image modality, its patch-wise biomarkers were feed to a single DNN. The features from these 6 DNNs were fused by another DNN to generate the final classification result.

- Unsupervised Pre-training** For unsupervised pre-training step, each DNN was trained as a stacked-autoencoder(SAE). Autoencoder is an artificial neural network used for unsupervised learning of non-linear hidden patterns from input data. It consists of three layers, input layer, hidden layer and output layer, for which two nearby layers are fully-connected. Three functions are used to define an autoencoder, encoding function, decoding function and loss function. In this study, encoding function is defined as: $y = s(W_1x + b_1)$, where x is the input data, y is the latent representation, W_1 is the weight matrix, b_1 is the bias term and s is the activation function for which we used rectified linear function $\max(0, x)$. Similarly, decoding function can be represented as: $z = s(W_2y + b_2)$, where we constrained it with tied weight $W_1 = W_2^T$ and z is the reconstructed data which is supposed to be close to input x . Squared error $\frac{1}{2}||x - z||^2$ is applied as loss function to optimize the network. The hypothesis is that the latent representation can capture the main factors of variation in the data. Comparing with another popular unsupervised feature learning method principle component analysis (PCA), the activation function enables the network to capture non-linear factors of data variation, especially when multiple encoders and decoders are stacked to form a SAE. To fully train the network, we applied greedy layer wise training²⁶ approach where every hidden layer was trained separately.
- Supervised Fine-tuning** After pre-training, the first three layers of a DNN were initialized with the parameters of encoders from pre-trained SAE followed by a softmax output layer. At first we trained the output layer independently while fixing the parameters of first 3 layers. Then we fine-tuned the whole network as Multilayer Perceptron (MLP) with subject labels for criterion. The network outputs the probabilities of a subject belongs to each class and the class with highest probability determines the output label of the subject. If we use x^i, y^i to represent the input feature vector and label of the i_{th} sample, respectively, the loss function based on cross entropy can be displayed as:

$$H(i) = -\frac{1}{N} \sum_{i=1}^N \sum_{j=1}^2 [\mathbb{1}\{y^i = j\} \log(h(x^i)_j)] \quad (1)$$

where N is the number of input samples, j represents the class of samples, and h represents the network function.

- Optimization of Network** Every training step of the networks were performed via back propagation with Adam algorithm²⁷. It is a first-order gradient-based optimization algorithm which has been proven to be computational efficient and appropriate for training deep neural network. During training stage, the training set was randomly split into mini

batches²⁸ where each of them contains 50 samples in this study. At every iteration, only a single mini batch was used for optimization. After every batch has been used once, the training set was reordered and randomly divided again so that each batch would have different samples in different epoch.

- **Dropout** In order to prevent deep neural network from overfitting, regularization is necessary to reduce its generalization error. In this study, we used dropout²⁹ to learn more robust features and prevent overfitting. In the dropout layer, some units were randomly dropped, providing a way to combine exponentially many different neural networks. In this study, we inserted dropout layers after every hidden layer. In each iteration of training stage, only half of hidden units were randomly selected to feed the results to the next layer, while in the testing stage all hidden units were kept to perform the classification. By avoiding training all hidden units on every training sample, this regularization technique not only prevented complex co-adaptations on training data and decrease overfitting, but also reduced the amount of computation and improved training speed.
- **Early Stopping** Another approach we used to prevent overfitting is early stopping. Because deep architecture were trained with iterative back propagation, the network were prone to be more adaptive to training data after every epoch. At a certain point, improving the network's fit to the training set will start to decrease generalization accuracy. In order to terminate the optimization algorithm before over-fitting, early stopping was used to provide guidance for how many iterations are needed. In the cross validation experiment, after dividing the data set into training and testing, we further split the training samples into a training set and a validation set. The networks were trained only with data in the former set, while samples in the latter set was used to determine when to stop the algorithm: while the network has the highest generalization accuracy for validation set. In actual training, we stopped the optimization if the validation accuracy had ceased to increase for 50 epochs.
- **Ensemble Classifiers** Although early stopping has proven to be useful in most deep learning problems, relatively small data set limited the number of samples we could use for validation. And a small validation set may not able to represent the whole data set resulting in a biased network. Therefore, we resorted to ensemble multiple classifiers to perform more stable and robust classification. Instead of selecting a single validation set, we randomly divided the training set into 10 sets and used them to train 10 different networks to 'vote' for the classification. At the training stage, for network i , set i would be used for validation while the rest 9 sets were used for training. At the testing stage, the test samples were feed into all these networks resulting in 10 sets of probabilities. For each sample, the probabilities from 10 networks was added and the class with highest probability was the classification result of this sample. Although the performance of ensemble classifiers may not be better than single network in every occasion, this strategy can statistically improve the classification accuracy as well as the robustness and stability of the classifier.

Results and Discussion

Experiments Setup

The proposed deep neural network was built with Tensorflow³⁰, an open source deep learning toolbox provided by Google. First, to compare the discriminant ability with state-of-the-art methods, 10-fold cross validation experiments were applied to classify sMCI and pMCI subjects. Then we performed three experiments with different training sets to test whether the images of pNC and pMCI contain AD pathology or not. For these experiments, 4 data sets: sNC, sAD, pNC and pMCI, were divided into two groups in 3 different ways: 1) subjects of sNC and sAD were considered as group 1, and subjects of pNC and pMCI belonged to group 2; 2) subjects of pMCI, sNC and sAD belonged to group1, and pNC were considered as group2; 3) all subjects were considered as group1. For each experiment, we applied a 10-fold cross validation on group1. The subjects of group 1 were randomly divided into 10 subsets, with 9 sets used for training and the rest set combined with subjects of group 2 used for testing. As detailed in the Methods Section, 10% of training subjects were randomly selected as validation set for early stopping to prevent overfitting. 10 networks with different validation set were trained to 'vote' for the final classification result. Noticing it was not images but subjects we were splitting, so images from different time point of the same subject won't be used for both training and testing.

Compare with State-of-the-Art Methods

Researchers in the past have worked on classification of subjects with progressive cognitive decline and those with stable cognitive impairment. pMCI were recognized as individuals with high risk of AD, while the sMCI were considered as those with no risk or low risk of AD in these studies. To evaluate the performance of our approach, we compared the classification accuracy of pMCI vs. sMCI with previous methods using the same data modality, i.e. T1-weighted MRI and FDG-PET^{13, 18, 31, 32}. The proposed network outperformed the state-of-the-art method in classifying pMCI and sMCI individuals, irrespective of using single or multimodal imaging, as shown in Table 2. It is worth to mention that in the study of Chen et.al³², they performed

domain transfer learning to exploit the auxiliary domain data(AD/NC subjects) to improve the classification. Even though, the accuracy of our methods without auxiliary knowledge was 3.5% accuracy than theirs.

Method	Modality	# Subjects	Accuracy	Sensitivity	Specificity
Young et al.	MRI	143	64.3	53.2	69.8
Liu et al.	MRI	234	68.8	64.29	74.07
Suk et al.	MRI	204	72.42	36.7	90.98
Cheng et al.	MRI	99	73.4	74.3	72.1
Proposed	MRI	626	75.44	77.27	76.19
Young et al.	PET	143	65.0	66.0	64.6
Liu et al.	PET	234	68.8	57.14	82.41
Suk et al.	PET	204	70.75	25.45	96.55
Cheng et al.	PET	99	71.6	76.4	67.9
Proposed	PET	626	81.53	78.20	82.47
Young et al.	MRI+PET+APOE	143	69.9	78.7	65.6
Liu et al.	PET+MRI	234	73.5	76.19	70.37
Suk et al.	PET+MRI	204	75.92	48.04	95.23
Cheng et al.	PET+MRI+CSF	99	79.4	84.5	72.7
Proposed	PET+MRI	626	82.93	79.69	83.84

Table 2. Accuracy(%), Sensitivity(%), and Specificity(%) of the proposed network comparing with state-of-the-art methods. The third row is the number of subjects used in the experiments

AD Pathology Classification

One problem of sMCI subjects was that we only know they remained stable at the time of preparation this manuscript, but they could still progress to AD or other mental disease in the future. Although the the sMCI vs. pMCI experiment were commonly used to test the discriminate ability of classifiers in recent studies, the classification result of sMCI subjects may not be very accurate. Therefore, we performed the second experiment involved classifying individuals with only known Alzheimer’s progression (pNC, pMCI and sAD) and normal controls (sNC). We investigated the performance of the classifier by using various combinations of samples during training phase. At a very basic level, we trained the classifier by discriminating sAD and sNC, at the next level pMCI and sAD were combined to represent the Alzheimer’s group and trained to discriminate them from the sNC group. In the last level we combined pNC, pMCI and sAD to represent the Alzheimer’s group to discriminate from the sNC group. The features extracted by the deep neural network are displayed in Fig 3. We observed the accuracy and sensitivity of the classifier progressively improved by additionally training with pMCI and pNC, while the specificity decreased, as displayed in Table 4. Further, the classifier performance was marginally better with the combination of FDG-PET and structural measurements compared to the performances with individual modalities. Interestingly, the classifier performance of structural imaging measurements were inferior to that of FDG-PET measurements. Supporting, the fact that FDG-PET, a measure of neuronal activity is a better tool to identify prodromal Alzheimer’s as compared to structural images^{33,34}.

Multiscale Classification

The classification accuracy of features extracted with different scales are listed in Table 3. We could not recognize any trend of increasing or decreasing classification performance with the changes in patch size. Therefore, features with higher resolution do not necessarily cover the discriminative information of lower resolution features. However, fusing multiscale features yielded superior accuracy as compared to uniscale, suggesting the network has the ability to capture discriminative information across the coarse to fine resolutions.

Early Diagnosis

We also investigated the classifier’s ability to identify individuals with high risk of acquiring Alzheimer’s, prior to disease onset. The classifier trained with the combined sample of Alzheimer’s trajectory (pNC, pMCI and sAD) was superior, as compared to the classifier trained with sAD alone. As the network classifier was trained with patterns of AD trajectory using pNC and pMCI, the network was able to achieve exceptional classification performances in identifying individuals with AD risk, i.e the classifier recognized individuals with AD risk with a of 90.08%, 85.61% and 81.20%, approximately at 1, 2, and 3 years prior to disease onset respectively. Studies in the past have predicted AD onset, using unimodal or multimodal investigation. Few studies have used PET as a single modality or in combination with structural MRI, CSF or cognitive measures to predict

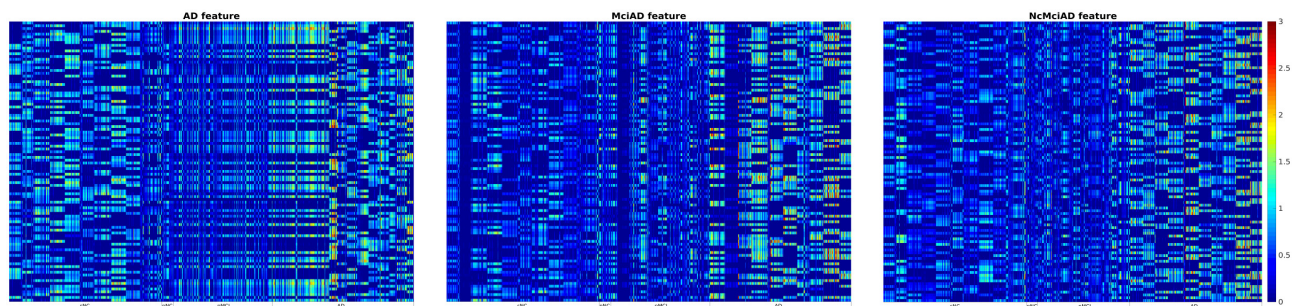


Figure 3. Features fed to the output layer. From left to right the training set is sNC vs sAD, sNC vs sAD and pMCI, and sNC vs sAD, pMCI and pNC, respectively. The y axis represents the units of the second from last layer, while x axis denotes the different data samples. This figure shows the different patterns as distilled by the deep learning network from the sNC, pNC, pMCI and AD images.

Training Set	Modality	500	1000	2000	Multiscale
sAD vs. sNC	FDG-PET	84.29	83.76	83.89	84.46
	MRI	81.27	81.58	81.01	81.89
sAD and pMCI vs. sNC	FDG-PET	85.34	84.80	84.87	85.46
	MRI	82.18	82.69	82.10	82.77
sAD, pMCI and pNC vs. sNC	FDG-PET	85.43	85.28	84.93	85.89
	MRI	81.69	82.04	81.64	82.45

Table 3. Accuracy(%) using features at different scales of different modality.

AD onset^{13,32,35-38}. The accuracy of 3 year prediction in the present network analysis was superior than those reported in the quoted studies. Studies predicting the illness onset, using structural MRI as a standalone tool or in addition to other clinical variables, have reported accuracy values inferior than to those obtained using PET^{5,39-49}.

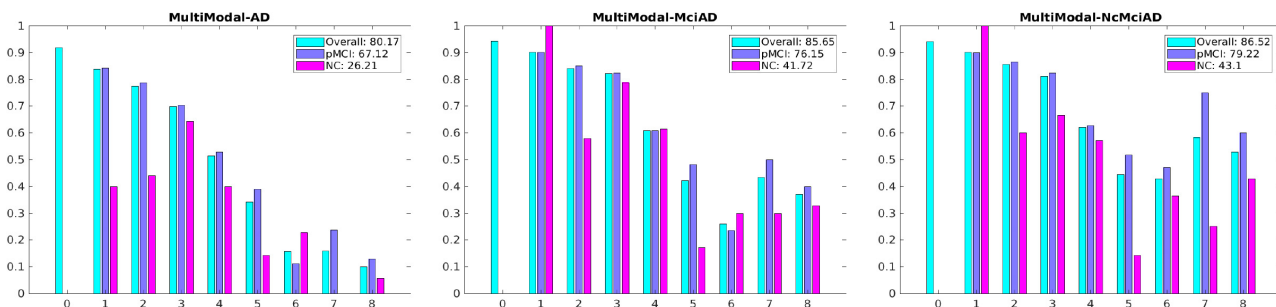


Figure 4. Classification accuracy of different training sets. From left to right the training set is sNC vs sAD, sAD and pMCI, sAD, pMCI and pNC, respectively. The y axis represents accuracy, while x axis denotes time(year) to conversion in which '0' means the subjects are already diagnosed as AD at the imaging visit. The number in legend is the classification accuracy of all time points. Noticing the accuracy increases with more data used for training.

Deep neural network is a strong tool for accurate recognition of objects, by a-priori training of images with well characterized objects. Hence the basic requirement for accurate classification using DNN tool are providing large number of images (usually in millions) and well characterized objects during supervised training phase¹⁵. Therefore a compromise in the a-priori knowledge of the objects (features of Alzheimer's) provided during training would limit the accuracy of the subsequent classification. As our current understanding of AD pathogenesis and its precise characteristics in FDG-PET and structural MRI images are limited, DNN suffered jeopardy in achieving 100% accurate classification. The clinical criteria for the diagnosis of AD involves a series of evaluations to provide near precise diagnosis. Despite rigorous evaluations, clinically diagnosed individuals with AD are not 100% accurate and hence the FDG-PET and structural MRI characters can overlap with conditions other than AD,

Training Set	FDG-PET			Volume			Multimodal		
	Acc	Sen	Spe	Acc	Sen	Spe	Acc	Sen	Spe
sAD vs. sNC	84.46	79.89	91.90	81.89	75.49	92.30	84.59	80.17	91.77
sAD and pMCI vs. sNC	85.46	85.01	86.19	82.77	79.76	87.65	85.96	85.65	86.45
sAD, pMCI and pNC vs. sNC	85.89	85.62	86.32	82.45	80.23	86.06	86.44	86.52	86.32

Table 4. Accuracy(%), sensitivity(%) and specificity(%) of different modality using different training sets.

including NC. Therefore the DNN trained with less accurately characterized images (FDG-PET and structural MRI) was unable to achieve 100% accurate classification. We propose an improvement in characterization of AD features by either upgrading FDG-PET and structural imaging methods or an increment in the understanding of AD specific pathogenesis, would positively impact the classification accuracy of the DNN classifier tool in future studies.

Conclusion

In summary, we proposed a deep neural network to identify individuals at risk of developing Alzheimer’s disease. We trained the classifier with patterns hidden in different resolutions and different modalities to distinguish subjects with Alzheimer’s trajectory (pNC, pMCI and sAD) and those without cognitive deficits (sNC). Our results show the classifier’s ability to successfully distinguish individuals with AD pathology from sNC with a remarkable accuracy of 82.93% using cross validation experiments. We observed the performance of network classifier built by the combination of FDG-PET and structural MRI images was better than those built with either structural MRI or FDG-PET alone. Further the classifier trained with the combined sample of pNC, pMCI and sAD (Alzheimer’s trajectory) was found to yield the highest classification accuracy. Lastly, our experiment to recognize individuals with AD pathology, prior to illness onset demonstrated a sensitivity of 85.68% in 3 years earlier to illness onset. Hence, the proposed deep neural network classifier can be a potential tool of choice in the future for early prediction of AD pathology. The number of pNC subjects was limited in this study resulting in a relatively low accuracy for pNC, as more data is accumulated in the future, we expect better accuracy in the prediction of NC subjects with AD pathology.

References

1. Association, A. *et al.* 2011 alzheimer’s disease facts and figures. *Alzheimer’s & dementia: journal Alzheimer’s Assoc.* **7**, 208 (2011).
2. Petersen, R. C. *et al.* Mild cognitive impairment: ten years later. *Arch. neurology* **66**, 1447–1455 (2009).
3. Brookmeyer, R., Johnson, E., Ziegler-Graham, K. & Arrighi, H. M. Forecasting the global burden of alzheimer’s disease. *Alzheimer’s & dementia* **3**, 186–191 (2007).
4. Weiner, M. W. *et al.* Recent publications from the Alzheimer’s Disease Neuroimaging Initiative: Reviewing progress toward improved AD clinical trials. *Alzheimers Dement* **13**, e1–e85 (2017).
5. Davatzikos, C., Bhatt, P., Shaw, L. M., Batmanghelich, K. N. & Trojanowski, J. Q. Prediction of mci to ad conversion, via mri, csf biomarkers, and pattern classification. *Neurobiol. aging* **32**, 2322–e19 (2011).
6. Landau, S. M. *et al.* Associations between cognitive, functional, and fdg-pet measures of decline in ad and mci. *Neurobiol. aging* **32**, 1207–1218 (2011).
7. Mosconi, L. *et al.* Pre-clinical detection of alzheimer’s disease using fdg-pet, with or without amyloid imaging. *J. Alzheimer’s Dis.* **20**, 843–854 (2010).
8. Farhan, S., Fahiem, M. A. & Tauseef, H. An ensemble-of-classifiers based approach for early diagnosis of alzheimer’s disease: Classification using structural features of brain images. *Comput. mathematical methods medicine* **2014** (2014).
9. Korolev, S., Safiullin, A., Belyaev, M. & Dodonova, Y. Residual and plain convolutional neural networks for 3d brain mri classification. *arXiv preprint arXiv:1701.06643* (2017).
10. Payan, A. & Montana, G. Predicting alzheimer’s disease: a neuroimaging study with 3d convolutional neural networks. *arXiv preprint arXiv:1502.02506* (2015).
11. Gray, K. R. *et al.* Multi-region analysis of longitudinal fdg-pet for the classification of alzheimer’s disease. *NeuroImage* **60**, 221–229 (2012).

12. Toussaint, P.-J. *et al.* Resting state fdg-pet functional connectivity as an early biomarker of alzheimer's disease using conjoint univariate and independent component analyses. *Neuroimage* **63**, 936–946 (2012).
13. Young, J. *et al.* Accurate multimodal probabilistic prediction of conversion to alzheimer's disease in patients with mild cognitive impairment. *NeuroImage: Clin.* **2**, 735–745 (2013).
14. Zhang, D. *et al.* Multimodal classification of alzheimer's disease and mild cognitive impairment. *Neuroimage* **55**, 856–867 (2011).
15. Krizhevsky, A., Sutskever, I. & Hinton, G. E. Imagenet classification with deep convolutional neural networks. In *Advances in neural information processing systems*, 1097–1105 (2012).
16. Liu, S. *et al.* Multimodal neuroimaging feature learning for multiclass diagnosis of alzheimer's disease. *IEEE Transactions on Biomed. Eng.* **62**, 1132–1140 (2015).
17. Liu, S. *et al.* Early diagnosis of alzheimer's disease with deep learning. In *Biomedical Imaging (ISBI), 2014 IEEE 11th International Symposium on*, 1015–1018 (IEEE, 2014).
18. Suk, H.-I., Lee, S.-W., Shen, D., Initiative, A. D. N. *et al.* Hierarchical feature representation and multimodal fusion with deep learning for ad/mci diagnosis. *NeuroImage* **101**, 569–582 (2014).
19. Zhang, W., Zelinsky, G. & Samaras, D. Real-time accurate object detection using multiple resolutions. In *Computer Vision, 2007. ICCV 2007. IEEE 11th International Conference on*, 1–8 (IEEE, 2007).
20. Lowe, D. G. Distinctive image features from scale-invariant keypoints. *Int. journal computer vision* **60**, 91–110 (2004).
21. Tang, Y. & Mohamed, A.-r. Multiresolution deep belief networks. In *AISTATS*, 1203–1211 (2012).
22. Dale AM, S. M., Fischl B. Cortical surface-based analysis. ii: Inflation, flattening, and a surface-based coordinate system. *Neuroimage* **9(2)**, 195–207 (1999).
23. Raamana, P. R. *et al.* Thickness network features for prognostic applications in dementia. *Neurobiol. aging* **36**, S91–S102 (2015).
24. Younes, M. B. M. M. A. T. L. Computing large deformation metric mappings via geodesic flows of diffeomorphisms. *Int. journal computer vision* **61.2**, 139–157 (2005).
25. Jenkinson, M., Bannister, P., Brady, M. & Smith, S. Improved optimization for the robust and accurate linear registration and motion correction of brain images. *Neuroimage* **17**, 825–841 (2002).
26. Bengio, Y., Lamblin, P., Popovici, D., Larochelle, H. *et al.* Greedy layer-wise training of deep networks. *Adv. neural information processing systems* **19**, 153 (2007).
27. Kingma, D. & Ba, J. Adam: A method for stochastic optimization. *arXiv preprint arXiv:1412.6980* (2014).
28. Bengio, Y. Practical recommendations for gradient-based training of deep architectures. In *Neural networks: Tricks of the trade*, 437–478 (Springer, 2012).
29. Srivastava, N., Hinton, G. E., Krizhevsky, A., Sutskever, I. & Salakhutdinov, R. Dropout: a simple way to prevent neural networks from overfitting. *J. Mach. Learn. Res.* **15**, 1929–1958 (2014).
30. Abadi, M., Agarwal, A., Barham, P., Brevdo, E. & *et al.* TensorFlow: Large-scale machine learning on heterogeneous systems (2015). URL <http://tensorflow.org/>. Software available from tensorflow.org.
31. Liu, K., Chen, K., Yao, L. & Guo, X. Prediction of mild cognitive impairment conversion using a combination of independent component analysis and the cox model. *Front. human neuroscience* **11** (2017).
32. Cheng, B., Liu, M., Zhang, D., Munsell, B. C. & Shen, D. Domain transfer learning for mci conversion prediction. *IEEE Transactions on Biomed. Eng.* **62**, 1805–1817 (2015).
33. Kawachi, T. *et al.* Comparison of the diagnostic performance of FDG-PET and VBM-MRI in very mild Alzheimer's disease. *Eur. J. Nucl. Medicine Mol. Imaging* **33**, 801–809 (2006).
34. Chételat, G. *et al.* Direct voxel-based comparison between grey matter hypometabolism and atrophy in Alzheimer's disease. *Brain* **131**, 60–71 (2008).
35. Xu, L., Wu, X., Chen, K. & Yao, L. Multi-modality sparse representation-based classification for alzheimer's disease and mild cognitive impairment. *Comput. methods programs biomedicine* **122**, 182–190 (2015).
36. Cabral, C. *et al.* Predicting conversion from mci to ad with fdg-pet brain images at different prodromal stages. *Comput. biology medicine* **58**, 101–109 (2015).

37. Zhang, D. & Shen, D. Predicting future clinical changes of MCI patients using longitudinal and multimodal biomarkers. *PLoS ONE* **7**, e33182 (2012).
38. Shaffer, J. L. *et al.* Predicting cognitive decline in subjects at risk for Alzheimer disease by using combined cerebrospinal fluid, MR imaging, and PET biomarkers. *Radiol.* **266**, 583–591 (2013).
39. Eskildsen, S. F., Coupe, P., Garcia-Lorenzo, D., Fonov, V. & *et al.* Prediction of Alzheimer’s disease in subjects with mild cognitive impairment from the ADNI cohort using patterns of cortical thinning. *Neuroimage* **65**, 511–521 (2013).
40. Moradi, E. *et al.* Machine learning framework for early mri-based alzheimer’s conversion prediction in mci subjects. *Neuroimage* **104**, 398–412 (2015).
41. Korolev, I. O., Symonds, L. L., Bozoki, A. C., Initiative, A. D. N. *et al.* Predicting progression from mild cognitive impairment to alzheimer’s dementia using clinical, mri, and plasma biomarkers via probabilistic pattern classification. *PLoS one* **11**, e0138866 (2016).
42. Misra, C., Fan, Y. & Davatzikos, C. Baseline and longitudinal patterns of brain atrophy in MCI patients, and their use in prediction of short-term conversion to AD: results from ADNI. *Neuroimage* **44**, 1415–1422 (2009).
43. Ye, J. *et al.* Sparse learning and stability selection for predicting MCI to AD conversion using baseline ADNI data. *BMC Neurol* **12**, 46 (2012).
44. Gaser, C., Franke, K., Kloppel, S., Koutsouleris, N. & Sauer, H. BrainAGE in Mild Cognitive Impaired Patients: Predicting the Conversion to Alzheimer’s Disease. *PLoS ONE* **8**, e67346 (2013).
45. Cuingnet, R. *et al.* Automatic classification of patients with Alzheimer’s disease from structural MRI: a comparison of ten methods using the ADNI database. *Neuroimage* **56**, 766–781 (2011).
46. Wolz, R., Julkunen, V., Koikkalainen, J., Niskanen, E. & *et al.* Multi-method analysis of MRI images in early diagnostics of Alzheimer’s disease. *PLoS ONE* **6**, e25446 (2011).
47. Chupin, M., Gerardin, E., Cuingnet, R., Boutet, C. & *et al.* Fully automatic hippocampus segmentation and classification in Alzheimer’s disease and mild cognitive impairment applied on data from ADNI. *Hippocampus* **19**, 579–587 (2009).
48. Cho, Y., Seong, J. K., Jeong, Y., Shin, S. Y. & *et al.* Individual subject classification for Alzheimer’s disease based on incremental learning using a spatial frequency representation of cortical thickness data. *Neuroimage* **59**, 2217–2230 (2012).
49. Coupe, P., Eskildsen, S. F., Manjon, J. V., Fonov, V. S. & Collins, D. L. Simultaneous segmentation and grading of anatomical structures for patient’s classification: application to Alzheimer’s disease. *Neuroimage* **59**, 3736–3747 (2012).

Consortia

for the Alzheimer’s Disease Neuroimaging Initiative

Michael Weiner², Paul Aisen³, Ronald Petersen⁴, Clifford Jack⁵, William Jagust⁶, John Trojanowki⁷, Arthur Toga⁸, Laurel Beckett⁹, Robert Green¹⁰, Andrew Saykin¹¹, John Morris¹², Leslie Shaw¹², Jeffrey Kaye¹³, Joseph Quinn¹³, Lisa Silbert¹³, Betty Lind¹³, Raina Carter¹³, Sara Dolen¹³, Lon Schneider⁸, Sonia Pawluczyk⁸, Mauricio Beccera⁸, Liberty Teodoro⁸, Bryan Spann⁸, James Brewer¹⁴, Helen Vanderswag¹⁴, Adam Fleisher¹⁴, Judith Heidebrink¹⁵, Joanne Lord¹⁵, Sara Mason⁵, Colleen Albers⁵, David Knopman⁵, Kris Johnson⁵, Rachele Doody¹⁶, Javier Villanueva-Meyer¹⁶, Munir Chowdhury¹⁶, Susan Rountree¹⁶, Mimi Dang¹⁶, Yaakov Stern¹⁷, Lawrence Honig¹⁷, Karen Bell¹⁷, Beau Ances¹², John Morris¹², Maria Carroll¹², Mary Creech², Erin Franklin¹², Mark Mintun¹², Stacy Schneider¹², Angela Oliver¹², Daniel Marson¹⁸, Randall Griffith¹⁸, David Clark¹⁸, David Geldmacher¹⁸, John Brockington¹⁸, Erik Roberston¹⁸, Marissa Natelson Love¹⁸, Hillel Grossman¹⁹, Efe Mitsis¹⁹, Raj Shah²⁰, Leyla deToledo-Morrell²⁰, Ranjan Duara²¹, Daniel Varon²¹, Maria Greig²¹, Peggy Roberts²¹, Marilyn Albert²², Chiadi Onyike²², Daniel D’Agostino²², Stephanie Kielb²², James Galvin²³, Brittany Cerbone²³, Christina Michel²³, Dana Pogorelec²³, Henry Rusinek²³, Mony de Leon²³, Lidia Glodzik²³, Susan De Santi²³, P. Doraiswamy²⁴, Jeffrey Petrella²⁴, Salvador Borges-Neto²⁴, Terence Wong²⁴, Edward Coleman²⁴, Charles Smith²⁵, Greg Jicha²⁵, Peter Hardy²⁵, Partha Sinha²⁵, Elizabeth Oates²⁵, Gary Conrad²⁵, Anton Porsteinsson²⁶, Bonnie Goldstein²⁶, Kim Martin²⁶, Kelly Makino²⁶, M. Ismail²⁶, Connie Brand²⁶, Ruth Mulnard²⁷, Gaby Thai²⁷, Catherine Mc-Adams-Ortiz²⁷, Kyle Womack²⁸, Dana Mathews²⁸, Mary Quiceno²⁸, Allan Levey²⁹, James Lah²⁹, Janet Cellar²⁹, Jeffrey Burns³⁰, Russell Swerdlow³⁰, William Brooks³⁰, Liana Apostolova³¹, Kathleen Tingus³¹, Ellen Woo³¹, Daniel Silverman³¹, Po Lu³¹, George Bartzokis³¹, Neill Graf-Radford³², Francine Parftt³², Tracy Kendall³², Heather Johnson³², Martin Farlow¹¹, Ann Marie Hake¹¹, Brandy Matthews¹¹, Jared Brosch¹¹, Scott Herring¹¹, Cynthia Hunt¹¹, Christopher Dyck³³, Richard Carson³³, Martha MacAvoy³³, Pradeep Varma³³, Howard Chertkow³⁴, Howard Bergman³⁴, Chris Hosein³⁴, Sandra Black³⁵, Bojana Stefanovic³⁵, Curtis Caldwell³⁵, Ging-Yuek Robin Hsiung³⁶, Howard Feldman³⁶, Benita Mudge³⁶, Michele Assaly³⁶, Elizabeth Finger³⁷,

Stephen Pasternack³⁷, Irina Rachisky³⁷, Dick Trost³⁷, Andrew Kertesz³⁷, Charles Bernick³⁸, Donna Munic³⁸, Marek-Marsel Mesulam³⁹, Kristine Lipowski³⁹, Sandra Weintraub³⁹, Borna Bonakdarpour³⁹, Diana Kerwin³⁹, Chuang-Kuo Wu³⁹, Nancy Johnson³⁹, Carl Sadowsky⁴⁰, Teresa Villena⁴⁰, Raymond Scott Turner⁴¹, Kathleen Johnson⁴¹, Brigid Reynolds⁴¹, Reisa Sperling⁴², Keith Johnson⁴², Gad Marshall⁴², Jerome Yesavage⁴³, Joy Taylor⁴³, Barton Lane⁴³, Allyson Rosen⁴³, Jared Tinklenberg⁴³, Marwan Sabbagh⁴⁴, Christine Belden⁴⁴, Sandra Jacobson⁴⁴, Sherye Sirrel⁴⁴, Neil Kowall⁴⁵, Ronald Killiany⁴⁵, Andrew Budson⁴⁵, Alexander Norbash⁴⁵, Patricia Lynn Johnson⁴⁵, Thomas Obisesan⁴⁶, Saba Wolday⁴⁶, Joanne Allard⁴⁶, Alan Lerner⁴⁷, Paula Ogrocki⁴⁷, Curtis Tatsuoka⁴⁷, Parianne Fatica⁴⁷, Evan Fletcher⁴⁸, Pauline Maillard⁴⁸, John Olichney⁴⁸, Charles DeCarli⁴⁸, Owen Carmichael⁴⁸, Smita Kittur⁴⁹, Michael Borrie⁵⁰, T-Y Lee⁵⁰, RobBartha⁵⁰, Sterling Johnson⁵¹, Sanjay Asthana⁵¹, Cynthia Carlsson⁵¹, Steven Potkin⁵², Adrian Preda⁵², Dana Nguyen⁵², Pierre Tariot⁵³, Anna Burke⁵³, Nadira Trncic⁵³, Adam Fleisher⁵³, Stephanie Reeder⁵³, Vernice Bates⁵⁴, Horacio Capote⁵⁴, Michelle Rainka⁵⁴, Douglas Scharre⁵⁵, Maria Kataki⁵⁵, Anahita Adeli⁵⁵, Earl Zimmerman⁵⁶, Dzintra Celmins⁵⁶, Alice Brown⁵⁶, Godfrey Pearlson⁵⁷, Karen Blank⁵⁷, Karen Anderson⁵⁷, Laura Flashman⁵⁸, Marc Seltzer⁵⁸, Mary Hynes⁵⁸, Robert Santulli⁵⁸, Kaycee Sink⁵⁹, Leslie Gordineer⁵⁹, Jef Williamson⁵⁹, Pradeep Garg⁵⁹, Franklin Watkins⁵⁹, Brian Ott⁶⁰, Henry Querfurth⁶⁰, Geoffrey Tremont⁶⁰, Stephen Salloway⁶¹, Paul Malloy⁶¹, Stephen Correia⁶¹, Howard Rosen⁶², Bruce Miller⁶², David Perry⁶², Jacobo Mintzer⁶³, Kenneth Spicer⁶³, David Bachman⁶³, Nunzio Pomara⁶⁴, Raymundo Hernando⁶⁵, Antero Sarrael⁶⁴, Norman Relkin⁶⁵, Gloria Chaing⁶⁵, Michael Lin⁶⁵, Lisa Ravdin⁶⁵, Amanda Smith⁶⁶, Balebail Ashok Raj⁶⁶ & Kristin Fargher⁶⁶.

²Magnetic Resonance Unit at the VA Medical Center and Radiology, Medicine, Psychiatry and Neurology, University of California, San Francisco, USA. ³San Diego School of Medicine, University of California, California, USA. ⁴Mayo Clinic, Minnesota, USA. ⁵Mayo Clinic, Rochester, USA. ⁶University of California, Berkeley, USA. ⁷University of Pennsylvania, Pennsylvania, USA. ⁸University of Southern California, California, USA. ⁹University of California, Davis, California, USA. ¹⁰MPH Brigham and Women's Hospital/Harvard Medical School, Massachusetts, USA. ¹¹Indiana University, Indiana, USA. ¹²Washington University St. Louis, Missouri, USA. ¹³Oregon Health and Science University, Oregon, USA. ¹⁴University of California–San Diego, California, USA. ¹⁵University of Michigan, Michigan, USA. ¹⁶Baylor College of Medicine, Houston, State of Texas, USA. ¹⁷Columbia University Medical Center, South Carolina, USA. ¹⁸University of Alabama – Birmingham, Alabama, USA. ¹⁹Mount Sinai School of Medicine, New York, USA. ²⁰Rush University Medical Center, Rush University, Illinois, USA. ²¹Wien Center, Florida, USA. ²²Johns Hopkins University, Maryland, USA. ²³New York University, NY, USA. ²⁴Duke University Medical Center, North Carolina, USA. ²⁵University of Kentucky, Kentucky, USA. ²⁶University of Rochester Medical Center, NY, USA. ²⁷University of California, Irvine, California, USA. ²⁸University of Texas Southwestern Medical School, Texas, USA. ²⁹Emory University, Georgia, USA. ³⁰University of Kansas, Medical Center, Kansas, USA. ³¹University of California, Los Angeles, California, USA. ³²Mayo Clinic, Jacksonville, Jacksonville, USA. ³³Yale University School of Medicine, Connecticut, USA. ³⁴McGill University, Montreal-Jewish General Hospital, Montreal, Canada. ³⁵Sunnybrook Health Sciences, Ontario, USA. ³⁶U.B.C. Clinic for AD & Related Disorders, Vancouver, BC, Canada. ³⁷Cognitive Neurology - St. Joseph's, Ontario, USA. ³⁸Cleveland Clinic Lou Ruvo Center for Brain Health, Ohio, USA. ³⁹Northwestern University, San Francisco, USA. ⁴⁰Premiere Research Inst (Palm Beach Neurology), west Palm Beach, USA. ⁴¹Georgetown University Medical Center, Washington DC, USA. ⁴²Brigham and Women's Hospital, Massachusetts, USA. ⁴³Stanford University, California, USA. ⁴⁴Banner Sun Health Research Institute, Sun City, AZ 85351, USA. ⁴⁵Boston University, Massachusetts, USA. ⁴⁶Howard University, Washington DC, USA. ⁴⁷Case Western Reserve University, Ohio, USA. ⁴⁸University of California, Davis – Sacramento, California, USA. ⁴⁹Neurological Care of CNY, Liverpool, NY 13088, USA. ⁵⁰Parkwood Hospital, Pennsylvania, USA. ⁵¹University of Wisconsin, Wisconsin, USA. ⁵²University of California, Irvine – BIC, USA. ⁵³Banner Alzheimer's Institute, Phoenix, AZ 85006, USA. ⁵⁴Dent Neurologic Institute, NY, USA. ⁵⁵Ohio State University, Ohio, USA. ⁵⁶Albany Medical College, NY, USA. ⁵⁷Hartford Hospital, Olin Neuropsychiatry Research Center, Connecticut, USA. ⁵⁸Dartmouth-Hitchcock Medical Center, New Hampshire, USA. ⁵⁹Wake Forest University Health Sciences, North Carolina, USA. ⁶⁰Rhode Island Hospital, state of Rhode Island, Providence, RI 02903, USA. ⁶¹Butler Hospital, Providence, Rhode Island, USA. ⁶²University of California, San Francisco, USA. ⁶³Medical University South Carolina, Charleston, SC 29425, USA. ⁶⁴Nathan Kline Institute, Orangeburg, New York, USA. ⁶⁵Cornell University, Ithaca, New York, USA. ⁶⁶USF Health Byrd Alzheimer's Institute, University of South Florida, Tampa, FL 33613, USA.

Acknowledgements

This work was supported by National Science Engineering Research Council (NSERC), Canadian Institutes of Health Research (CIHR), Michael Smith Foundation for Health Research (MSFHR), Brain Canada, Genome BC and the Pacific Alzheimer Research Foundation (PARF). Data collection and sharing for this project was funded by the Alzheimer's Disease Neuroimaging Initiative (ADNI) (National Institutes of Health Grant U01 AG024904) and DOD ADNI (Department of Defense award number W81XWH-12-2-0012). ADNI is funded by the National Institute on Aging, the National Institute of Biomedical Imaging and Bioengineering, and through generous contributions from the following: AbbVie, Alzheimer's Association; Alzheimer's

Drug Discovery Foundation; Araclon Biotech; BioClinica, Inc.; Biogen; Bristol-Myers Squibb Company; CereSpir, Inc.; Cogstate; Eisai Inc.; Elan Pharmaceuticals, Inc.; Eli Lilly and Company; EuroImmun; F. Hoffmann-La Roche Ltd and its affiliated company Genentech, Inc.; Fujirebio; GE Healthcare; IXICO Ltd.; Janssen Alzheimer Immunotherapy Research & Development, LLC.; Johnson & Johnson Pharmaceutical Research & Development LLC.; Lumosity; Lundbeck; Merck & Co., Inc.; Meso Scale Diagnostics, LLC.; NeuroRx Research; Neurotrack Technologies; Novartis Pharmaceuticals Corporation; Pfizer Inc.; Piramal Imaging; Servier; Takeda Pharmaceutical Company; and Transition Therapeutics. The Canadian Institutes of Health Research is providing funds to support ADNI clinical sites in Canada. Private sector contributions are facilitated by the Foundation for the National Institutes of Health (www.fnih.org). The grantee organization is the Northern California Institute for Research and Education, and the study is coordinated by the Alzheimer's Therapeutic Research Institute at the University of Southern California. ADNI data are disseminated by the Laboratory for Neuro Imaging at the University of Southern California.

Author contributions statement

Donghuan Lu and Weiguang Ding built the deep neural network. Donghuan Lu and Karteek Popuri processed the neuroimage data. Rakesh Balachander and Mirza Faisal Beg designed the experiments and interpreted the results. All authors reviewed the manuscript.

Additional information

Competing Interest: The authors declare that they have no competing interest.